

Design of Telescopic Soft Gripper for Mangosteen Harvesting

Kraiwit Thongprawit

Department of Mechanical and Mechatronics Engineering, Faculty of Engineering, Prince of Songkla University, Songkhla, Thailand
6510120019@email.psu.ac.th

Jutamane Auysakul

Department of Mechanical and Mechatronics Engineering, Faculty of Engineering, Prince of Songkla University, Songkhla, Thailand
jutamane.a@psu.ac.th (corresponding author)

Kunlapat Thongkaew

Department of Industrial and Manufacturing Engineering, Faculty of Engineering, Prince of Songkla University, Songkhla, Thailand
kunlapat.t@psu.ac.th

Chalita Hiransoog

Department of Mechanical and Mechatronics Engineering, Faculty of Engineering, Prince of Songkla University, Songkhla, Thailand
chalita.h@psu.ac.th

Charoenyutr Dechawayukul

Department of Mechanical and Mechatronics Engineering, Faculty of Engineering, Prince of Songkla University, Songkhla, Thailand
charoenyut.d@psu.ac.th

Received: 21 December 2024 | Revised: 16 January 2025 | Accepted: 24 January 2025

Licensed under a CC-BY 4.0 license | Copyright (c) by the authors | DOI: <https://doi.org/10.48084/etasr.10001>

ABSTRACT

This research presents a telescopic soft gripper designed to assist farmers in the harvesting of mangosteens. Subsequent to the outbreak of a pandemic, like the novel coronavirus (SARS-CoV-2), producers are encountering a workforce shortage during the harvesting of mangosteen. The labor crisis is currently becoming more acute, but the competition for mangosteen exports is increasing, requiring the expansion of mangosteen agricultural areas, which will ultimately give rise to a labor shortage. The gripper is fabricated from hyperelastic material, a material that offers flexibility and softness, making it ideal for delicate objects. Conventional soft grippers lack the telescopic design, which enables extension and retraction, allowing for the handling of various object sizes. The gripper's design optimization involved the evaluation of nine models with different internal inclinations and material thicknesses. Finite Element Analysis (FEA) was employed to simulate the deformation and stress responses. The optimized model, in comparison to nine other models, possesses a thickness of 2.25 mm and an internal inclination of 10 degrees, facilitating high deformation with acceptable stress. It has been demonstrated that the gripper can deform up to 132 mm, a finding that has been validated through experimentation. The experimental validation was conducted to corroborate these findings, demonstrating the gripper's capacity to securely grasp objects with diameters ranging from 50 mm to 70 mm and weights up to 22 N. Furthermore, the gripper's efficacy was assessed in a mangosteen harvesting scenario, where it demonstrated a capability to successfully harvest the fruit within a span of two seconds. The gripper's design is characterized by its compactness, low production cost, and ease of use, rendering it highly practical for agricultural applications in confined spaces. The telescopic soft gripper under consideration offers a versatile and scalable solution for

harvesting a wide range of crops of varying sizes, positioning it as a valuable tool for future agricultural automation.

Keywords-soft gripper; telescopic actuator; design pneumatic gripper; mangosteen harvesting

I. INTRODUCTION

Mangosteen is a significant agricultural product in Thailand, with China serving as its primary export market. However, by 2024, mangosteen exports to China had decreased compared to 2021. To maintain its market share, Thailand must increase export capacity and diversify export markets to reduce over-reliance on China. Expanding cultivation areas is essential to boost export potential but may lead to labor shortages in mangosteen harvesting in the near future. The integration of automation technology into contemporary agricultural practices has emerged as a fundamental strategy to enhance productivity, reduce manual labor, and ensure consistency and standardization in production [1]. Automated systems have profoundly transformed agricultural processes, enhancing efficiency in production, resource management, and harvesting when compared to traditional labor-intensive methods [2, 3]. This study explores the development of a soft gripper designed for mangosteen harvesting, with the aim of future integration into robotic arms. The usage of automation in the domain of fruit harvesting has been demonstrated to be a highly effective practice. Authors in [4] developed a berry-harvesting robot capable of picking berries in 9 seconds per berry, while authors in [5] successfully designed a robot for picking strawberries, with the capability to pick 710 strawberries per hour. Authors in [6] designed and developed a soft gripper consisting of a finger and a suction cup for harvesting apples, with a harvest rate of up to 70.77%. In a similar approach, authors in [7] have designed a 3D-printed soft gripper that is versatile enough to accommodate fruits of various sizes and shapes. Authors in [8] introduced a six-finger gripper designed for mango harvesting, capable of detaching and lifting fruits weighing up to 636 g. Similarly, authors in [9] developed telescopic fingers that can exert a thrust force of 8 N to 10 N on spherical objects, demonstrating their ability to lift objects of various sizes and weights. These experiments underscore the efficacy of telescopic fingers in securely gripping and lifting a diverse array of items. Additionally, authors in [10] designed a soft actuator capable of handling objects weighing up to 1,200 g, with a response time of less than two seconds, showcasing both speed and strength in handling tasks. These advancements underscore the growing potential of soft robotics in agricultural harvesting, particularly for tasks requiring precision, speed, and the ability to handle diverse object weights and shapes. The harvesting procedure necessitates the implementation of a gripper, which functions as an end effector affixed to the robot arm for the manipulation of objects. The grippers in question can be classified based on the actuator employed, which can be categorized into the following types: vacuum grippers [11-13], pneumatic grippers [14, 15], hydraulic grippers [16, 17], and electric grippers [18]. The fabrication of these grippers can be constructed with both rigid and soft materials, depending on the specific application requirements. Rigid grippers are distinguished by their robust structure and capacity to handle substantial weight. However, they are often designed for specific tasks and lack versatility [19]. Additionally, their

rigidity renders them ill-suited for tasks requiring delicacy and gentleness. Conversely, soft grippers offer distinct advantages, including a soft, flexible structure and lightweight design, which renders them ideal for delicate and precise objects [20]. While they demonstrate adaptability to object size, their weight-holding capacity is comparatively limited when compared to rigid grippers [21, 22].

In consideration of the aforementioned factors, soft grippers, including finger grippers [23, 24], tendon drive grippers [25, 26], universal grippers [27-29], and diaphragm grippers [30-31], have gained widespread application in harvesting operations due to their capacity to adapt to a diverse range of objects. Among these, the telescopic gripper merits particular attention due to its finger-like design, enabling it to extend and retract like a telescope. The mechanism of this gripper entails the usage of mechanical principles, encompassing the stretching and deflection of a flexible and corrugated structure. Its design is notable for its simplicity, a quality that facilitates easier manufacturing when compared to other gripper types. Its cost-effectiveness and retractable design render it suitable for disposable applications, particularly those involving infectious materials, hazardous substances, or objects in confined spaces. However, while these designs have achieved notable performance, they are not specifically optimized for the challenges associated with harvesting mangosteens. The latter require a gripper capable of handling fruits with varying sizes and fragile exteriors. This study builds upon the designs of authors in [9] and [15] by incorporating novel modifications to address these limitations. Specifically, the present study focuses on optimizing the gripper's internal angle and fold thickness, enhancing its telescopic displacement and grip efficiency for mangosteen harvesting. In contradistinction to the designs proposed before, which have been validated on lifting objects, our gripper has undergone specific testing for mangosteen harvesting, thereby demonstrating its capability to perform rapid, damage-free picks. These adaptations position the proposed gripper as a viable solution for expanding agricultural automation in mangosteen cultivation and beyond. The objective of this study is to design and develop a prototype of a soft gripper for mangosteen harvesting that uses a pneumatic system, defined as follows:

- It determines a suitable telescopic soft gripper based on compression elongation and stress values. To this end, a FEM model with various thicknesses and internal angles has been developed.
- The subsequent section will evaluate the efficiency of mangosteen harvesting with telescopic soft grippers in comparison to the harvesting time span of farmers.

The remainder of this paper is devoted to the FEM applied to hyperelastic materials using the Mooney-Rivlin model, with the simulation results and the optimized design of the telescopic finger. Furthermore, it describes the casting process

and the design of the rigid frame for the telescopic gripper while including all four evaluations performed to evaluate gripper performance: simulation validation, grip force testing, grasping of everyday objects, and mangosteen harvesting.

II. SIMULATION AND OPTIMIZED DESIGN OF THE TELESCOPIC ACTUATOR

The FEM is an approach that employs mathematical principles to address engineering challenges. It involves the assessment of how specific environmental factors influence the behavior of materials, such as structures, stress, strain, or force, to provide an approximate prediction of the problem's outcome. In this research, the FEM is implemented in conjunction with the MSC Marc Mentat Software (MSC) (version 2020.0.0) to optimize the deformation and stresses of the telescopic design.

A. Mooney–Rivlin Model

A variety of models are currently being developed to characterize the properties of hyperelastic materials. One such model is the Mooney-Rivlin model, which offers a simplified representation with fewer variables in its equations compared to other models. This model is particularly valuable for analyzing nonlinear materials and their behavior:

$$W = \sum_{i+j=1}^n C_{ijk}(I_1 - 3)^i(I_2 - 3)^j(I_3 - 1)^k + \sum_{i+j+k=1}^n \frac{1}{D_j}(J_{el} - 1)^{2i} \quad (1)$$

where W is the strain energy per unit volume, C_{ijk} is the material-specific constant, I_1 , I_2 , and I_3 are the three invariants of the Cauchy-Green deformation tensor, D_j is the incompressible property, and J_{el} is the elastic volume ratio.

B. Strain Energy Coefficient

The determination of the strain energy coefficient can be achieved by the experimental evaluation of the mechanical properties of hyperelastic materials, as shown in Figure 1. To determine the strain energy coefficient in (1), the uniaxial test is demonstrated and rewritten as:

$$W = \sum_{i+j=1}^n C_{ij}(I_1 - 3)^i(I_2 - 3)^j \quad (2)$$

where $J_{el} = 1$ and $I_3 = 0$ in case of fully incompressible material and I_1 , I_2 are defined as:

$$I_1 = \lambda_1^2 + \lambda_2^2 + \lambda_3^2 \quad (3)$$

$$I_2 = \lambda_1^2\lambda_2^2 + \lambda_2^2\lambda_3^2 + \lambda_1^2\lambda_3^2 \quad (4)$$

where λ_1 , λ_2 , and λ_3 represent the elongations of the element in three directions. The design of the telescopic actuator can be assumed to be incompressible by:

$$\lambda_1^2\lambda_2^2\lambda_3^2 = 1 \quad (5)$$

In the case of the uniaxial test, (5) contains $\lambda_1 = \lambda$, and $\lambda_2 = \lambda_3 = \lambda^{-1/2}$. Each direction's elongation depends on the amount of strain (ϵ), which can be expressed as follows:

$$\lambda = 1 + \epsilon \quad (6)$$

The stress (σ) of the hyperelastic material can be described using the C_{ij} parameter and elongation, as indicated by:

$$\sigma = 2[C_{10}(\lambda - \lambda^{-2}) + C_{01}(1 - \lambda^{-3} + 3C_{11}(\lambda^2 - \lambda - 1 + \lambda^{-2} + \lambda^{-3} - \lambda^{-4}))] \quad (7)$$

where σ signifies the normal stress, and C_{10} , C_{01} , and C_{11} are the strain energy coefficients of the Mooney-Rivlin model.



Fig. 1. Uniaxial testing machine.

C. Telescopic Design

The telescopic actuator is composed of an internal structure that functions as a chamber, which is actuated pneumatically, thereby enabling its extension and retraction capabilities. Furthermore, the interior angles can be modified to allow for bending when required. In its retracted state, the actuator maintains a compact form, rendering it particularly well-suited for storage and operation in confined spaces. The actuator's design and construction are economical. Fabricated from hyperelastic material, it is characterized by its softness, exceptional flexibility, durability against abrasion and tearing, shape stability, and suitability for harvesting applications. Figure 2 shows the telescopic design, which features a silicone rubber fold consisting of three layers. The present study, which is focused on the task of picking fruit, proposes an actuator design with a diameter of 90 mm and a height of 35 mm to grasp objects with dimensions between 50 mm and 70 mm. The optimized models demonstrate variations in thickness and internal angles, as presented in Figure 3. The application of pressure leads to the bending of the actuator, which is a consequence of its internal geometry. This augmentation of surface area during the harvesting process is a key advantage of the proposed design.

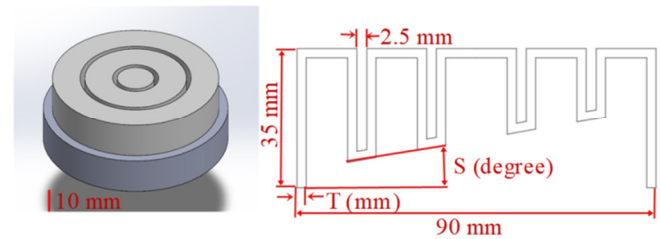


Fig. 2. Design of the telescopic actuator: 3D model (left), and 2D model (right).

D. Simulation Analysis

In this research, MSC for FEA was employed. To expedite the computational process, the object under investigation was designed with a planar configuration. To this end, a two-dimensional model and mesh were used, employing a quadrilateral mesh. As shown in Figure 3, the boundary conditions of the aforementioned planar model of the

optimized telescopic actuators are delineated. The analysis model employs the plane strain Full & Herrmann (Quad 80) formulation for solid structures. The research scope is hereby defined as follows: Firstly, the air pressure and atmospheric pressure are held constant. Secondly, the actuator is to be free of any leaks. Thirdly, the internal pressure is to maintain a constant distribution. In our research, the maximum pressure 1 and pressure 2 are set at 20 kPa, and we employed a linear ramp table to calculate the large strain of the static model. This calculation employed a constant time step of 0.02, consisting of 50 steps, and reported deformation and stress variations from the selected nodes.

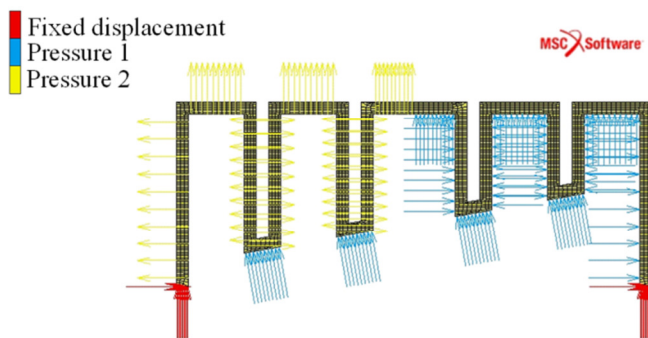


Fig. 3. Boundary conditions of the telescopic soft actuator.

Telescopic soft actuators are fabricated from materials with high tensile strength and significant deformation properties. For the purposes of this study, Dragon Skin 30 (Smooth-On, Inc., Macungie, PA, USA) was selected to produce the actuator. Tensile strength testing was conducted in accordance with ASTM D412 standards using a Z005 tensile testing machine (Zwick Roell, Ulm, Germany). The testing involved a 3 mm-thick silicone sample, which was tested at a speed of 500 mm/min until failure. The material testing results demonstrated a tensile strength of 2.5 MPa and an elongation at break of 311%, as shown in Figure 4. The strain energy coefficient was determined using MSC, employing the test results from specimen 3 of Dragon Skin 30, which is the average value when compared with other specimens. The model calculations yielded the following Mooney-Rivlin 3rd coefficients: $C_{10} = 1.146 \times 10^{-1}$ MPa, $C_{01} = 1.472 \times 10^{-8}$ MPa, and $C_{11} = 2.971 \times 10^{-2}$ MPa, with an error of 3.543×10^{-4} .

A correlation analysis reveals a clear trend between pressure and stretching distance when using a maximum pressure setting of 20 kPa. The thickness of the actuator exerts a substantial influence on the extent of stretching achieved. Thinner actuators exhibit superior stretchability in comparison to their thicker counterparts, as presented in Figure 5. This phenomenon can be attributed to the larger inertial material and cross-sectional area associated with thicker actuators, consequently leading to reduced levels of stress. Additionally, the angle of inclination has been found to have a significant impact on the extent of extension achieved. This relationship is examined across the three thickness levels in each internal inclination. It is evident that actuators with smaller angles demonstrate heightened stretchability. Conversely, actuators with larger angles, when subjected to pressure on inclined

surfaces, display a diminished capacity for extension, primarily attributable to deflection.

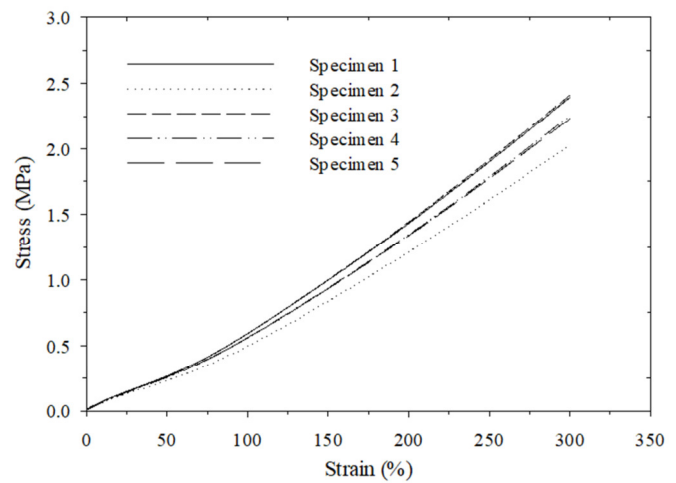


Fig. 4. The tensile strength test data.

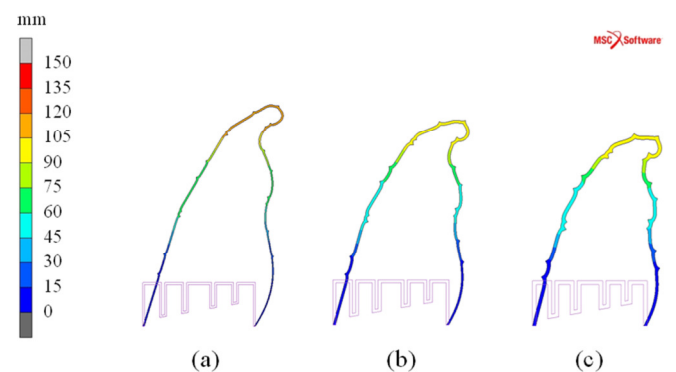


Fig. 5. Simulation results at an internal inclination of 10 degrees for models with thicknesses: (a) 1.5 mm, (b) 2.25 mm, and (c) 3 mm at 20 kPa.

The relationship between pressure and stress is demonstrated in the model, wherein the maximum pressure is set at 20 kPa. It was determined that the actuator, characterized by its reduced thickness, exhibited a high stress value. This is attributable to the actuator's diminished inertial and cross-sectional area, which are intrinsic components of its design. At an internal inclination of 15 degrees, the stress values for all three thicknesses increase, as pressure must exceed the friction of the folded actuator. This inclination is identified as a point where the influence of each thickness angle on tension becomes negligible. As presented in Figure 6, the simulation results demonstrate the outcomes for models with internal inclinations of 5 and 10 degrees, as well as a model with an internal inclination of 15 degrees. It is noteworthy that all models have a thickness of 2.25 mm and varying internal inclinations. Upon further examination, it was observed that models with internal inclinations of 5 and 10 degrees exhibited final stretch distances that were highly comparable to each other. Conversely, the model with an internal angle of 15 degrees demonstrates minimal elongation. This study is focused on the optimization of models with diverse thicknesses

and interior angles, with the objective of developing a model that is both suitable and accurate.

E. The Optimized Design of the Telescopic Actuator

As shown in Figure 7, Model 5, with a thickness of 2.25 mm and an inclination angle of 10 degrees, exhibited a stretch of 132 mm and a stress of 99 kPa at the final point when operated at 20 kPa. This model exhibited a moderate level of stretch and stress, leading to its selection for the fabrication of the actuator in this study.

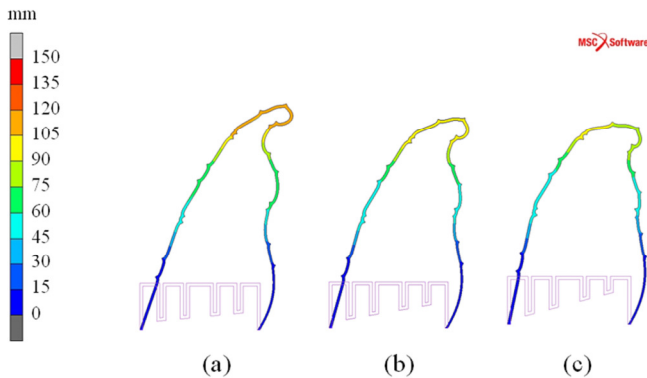


Fig. 6. Simulation results at thicknesses of 2.25 mm for models with internal inclination (a) of 5 degrees, (b) of 10 degrees, and (c) of 15 degrees at 20 kPa.

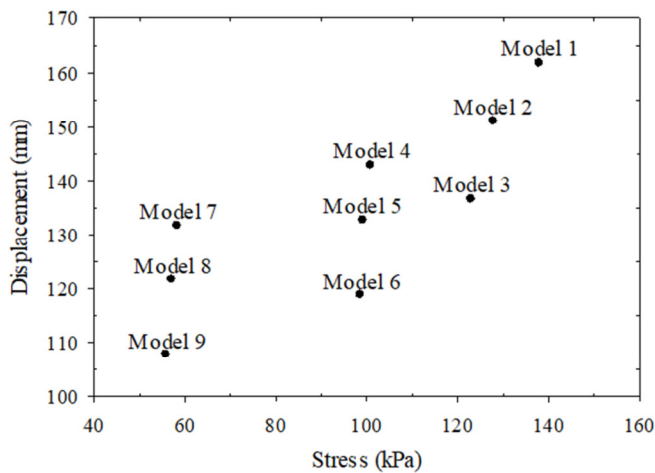


Fig. 7. Relationship between displacement and stress for all models.

III. MANUFACTURING PROCESS

A. Fabrication of the Telescopic Actuator

The telescopic actuator is fabricated through a casting process, necessitating the use of five molds, as presented in Figure 8. These molds comprise two circular bases that are securely fastened with screws, two detachable walls to facilitate disassembly, and a top cover with ventilation holes. These components serve the purpose of ensuring uniform layer formation by locking keyways and expelling any trapped air bubbles in the silicone. The molds are produced using a 3D printer, specifically the Flashforge Adventurer 3 (Zhejiang Flashforge 3D Technology Co., Ltd., Jinhua, China). These

components are designed for reusability and precision, ensuring a perfect fit for the internal inclination. During the assembly phase, the initial step involves securely connecting the mold base and walls, confirming the absence of any potential leaks. Subsequently, the Dragon Skin 30 mixture, comprising Part A and Part B, is poured into the mold in a 1:1 ratio based on the predetermined weight, as illustrated in Figure 8 (b). As a precautionary measure, an additional 10% of the expected weight is added to account for any potential silicone mold leaks. The silicone compound is thoroughly mixed, and air bubbles are eliminated using a vacuum chamber. The silicone mixture is then poured into the mold in a meticulous manner, as depicted in Figure 8 (c). Any air bubbles that emerge on the surface of the silicone are punctured with a pointed instrument after the mold has been meticulously rubbed and subsequently covered with the top plate, as illustrated in Figure 8 (d). Thereafter, the silicone is allowed to cure for a duration of 16 hours at room temperature.

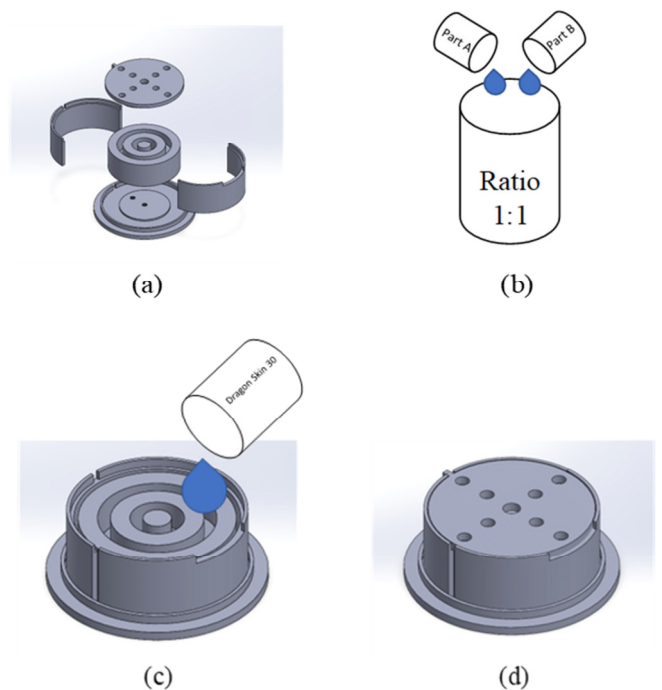


Fig. 8. Telescopic actuator fabrication process (a) 3D-printed model, (b) silicone preparation, (c) casting process, and (d) mold cover closure.

B. Design of the Rigid Frame

The configuration of the rigid frame is conceptualized to emulate the functionality of a human hand. The fabrication of this object is accomplished through the usage of 3D printing technology. The frame incorporates telescopic grippers, each comprising a mounting plate, gripper plate, and grip frame, as shown in Figure 9. The proposed design aims to facilitate the grasping of objects with diameters ranging from 50 to 70 mm. The mounting plate can be attached to the end of the Dobot CR5 robot arm with ease, enhancing its usability and enabling future experimentation.

IV. EXPERIMENTS AND RESULTS

This research is focused on the evaluation and validation of the performance of the telescopic actuator through four distinct tests. Firstly, the simulation results are validated. Secondly, a grasp force experiment is conducted. Thirdly, an experiment is carried out in which the actuator is used to grasp objects encountered in daily life. Finally, the harvesting of mangosteen is simulated. The validation of simulation results entails a comparative investigation of deformation, wherein the simulation and specimen results are meticulously examined to ascertain their concordance. The grasp force experiment is designed to scrutinize the tensile forces encountered during object extraction.

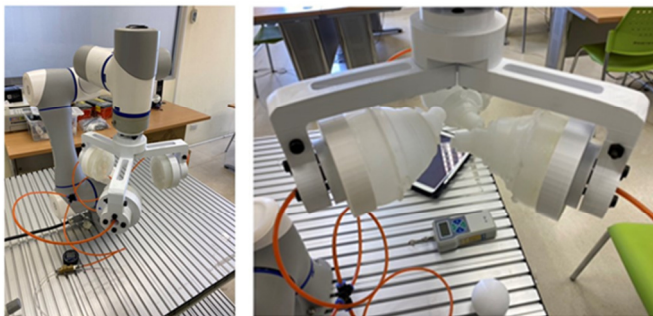


Fig. 9. Assembly of the rigid frame and the telescopic gripper: normal (left) and pressurized condition (right).

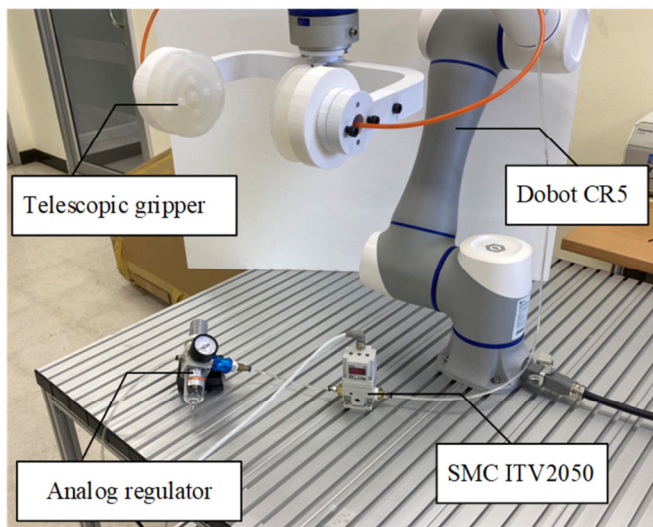


Fig. 10. The integration of the telescopic gripper into the robotic arm.

Subsequently, the daily life object grasping experiment was conducted to assess the grasping capabilities, encompassing the handling of various fruits and common items. The harvesting efficiency is then compared to that of farmers, with the time usage being a key metric. The telescopic gripper, a critical component of the robotic apparatus, is installed into a robot arm, as presented in Figure 10. Ensuring the precision and consistency of these tests necessitates precise control over air pressure. This control is maintained by using an analog air pressure controller, which has a pressure range of 0 to 50 kPa.

This controller regulates the air pressure to predefined values before it enters the SMC ITV2050 digital air pressure controller. The SMC ITV2050 boasts a wide pressure range of 0.005 MPa to 0.9 MPa and functions through a voltage divider circuit, enabling precise fine-tuning of the output voltage within the 0 to 10 V DC range. The precise regulation of this controller is facilitated by a potentiometer, ensuring that the gripper receives the requisite air pressure for optimal performance during testing.

A. Validation of the Simulation Results

In order to assess the accuracy and precision of the telescopic actuator, a comparison must be conducted between the deformation results from the simulation and those from the specimen testing. The objective of this experiment is to compare the gripper's elongation with the corresponding increment in air pressure. The air pressure from the control circuit should be adjusted in 5 kPa increments, ranging from 0 kPa to 15 kPa. The extension value is measured using the scale plate located at the rear of the test unit, as shown in Figure 11. Figure 12 presents a comparative analysis of the simulation results and the outcomes from two testing specimens. The telescopic actuator achieves a maximum height of 35 mm when inflated and extends up to 132 mm. The simulation indicates that the telescopic actuator stretches more quickly than was observed in the experiments. This discrepancy can be attributed to the friction between the folds in the real model, which is not accounted for in the analytical model. However, the maximum displacement at the tip of the telescopic actuator is similar between the simulation and experimental models. The observed discrepancies can be attributed to several factors, including the simulation's inability to predict defects that may emerge during the manufacturing and testing processes of a component, as well as material properties. Additionally, the presence of air bubbles within the workpiece during the manufacturing process has been identified as a critical factor that can lead to alterations in material properties. Consequently, the actuator's behavior and elongation characteristics undergo adjustments.

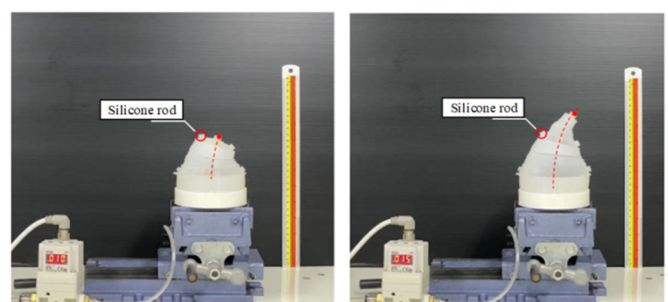


Fig. 11. The stretch at different air pressure levels: at 10 kPa (left), and at 15 kPa (right).

Furthermore, discrepancies in the thickness of the workpiece's walls can result in variations in elongation. The necessity of higher air pressure to overcome the inherent friction in the folded sections is a consequence of thicker walls, while thinner walls allow for greater stretching of the actuator. Furthermore, the presence of ventilation holes in the silicone mold can result in the formation of small silicone rods, as

presented in Figure 11. These rods contribute to the actuator exhibiting higher values than those predicted by the simulation model when fully stretched. These variations underscore the multifaceted nature of real-world manufacturing and testing, where numerous factors influence the actuator's performance, resulting in deviations from the idealized simulation results.

B. Grasp Force Experiment

This study examines the forces required to extract objects of varying shapes from the gripper and evaluates the gripper's resistance to forces encountered while handling diverse objects. The experimental setup involves two distinct phases, with the gripper subjected to a constant air pressure of 20 kPa throughout. The first phase involves testing different objects to evaluate the gripper's response to three different geometric shapes, including a cube, a cylinder, and a sphere with a diameter of 50 mm. The second phase involves a spherical object test, focusing exclusively on spherical objects resembling fruit, encompassing three different sizes: 50 mm, 60 mm, and 70 mm in diameter, respectively.

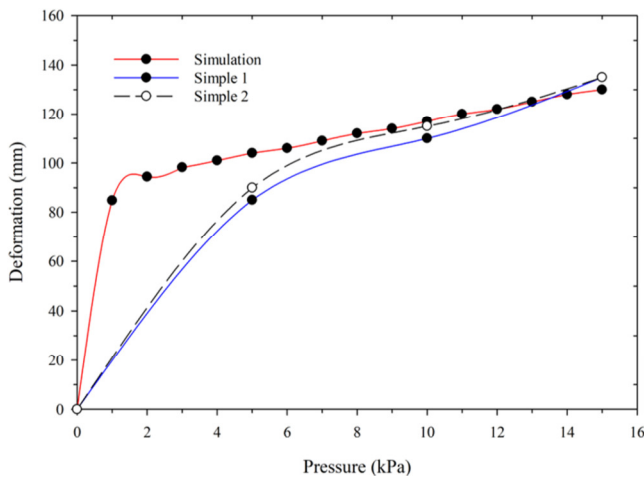


Fig. 12. Comparative analysis of deformation responses.

The gripper is used to grasp each spherical object, as shown in Figure 13. The force required for extraction is quantified using a digital force gauge (SF-100 Model, Wenzhou Sanhe Instrument Co., Ltd., Wenzhou, China). This comprehensive evaluation aims to provide insights into the telescopic gripper's ability to withstand force when interacting with objects of varying shapes and sizes, yielding valuable data for its practical applicability.

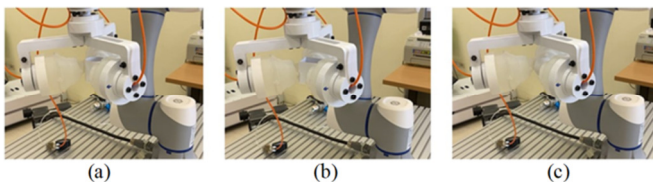


Fig. 13. Grasp force experiment (a) cylindrical shape, (b) cubic shape, and (c) spherical shape.

The test results for objects with a 50 mm size revealed distinct adhesive forces for various shapes, as presented in

Figure 14 (a). Among these, the cubic shape exhibited the highest adhesion force, registering at 16.5 N -22 N. The sphere shape exhibited an adhesion force of 16 N-19 N, while the cylinder shape exhibited a comparatively lower adhesion force of 15 N-19 N. This observed sequence in adhesion force can be attributed to the gripper's inherent deflection characteristics, which provide a larger adhesion surface when handling curved objects. However, when dealing with the 50 mm spherical and cylinder object, the limited size results in a minimal adhesion surface within the spherical space, consequently leading to a diminished tensile strength. In the subsequent phase of testing, which focuses on spherical objects, a distinct pattern emerges. As shown in Figure 14 (b), the 70-mm variant exhibited the highest adhesion force (24 N-26 N), followed by the 60-mm variant (19 N-22.5 N), and the 50-mm variant (16 N-19 N). This sequence corresponds to the notion that larger spherical shapes inherently provide more extensive contact surfaces, thereby enhancing their resistance to external forces.

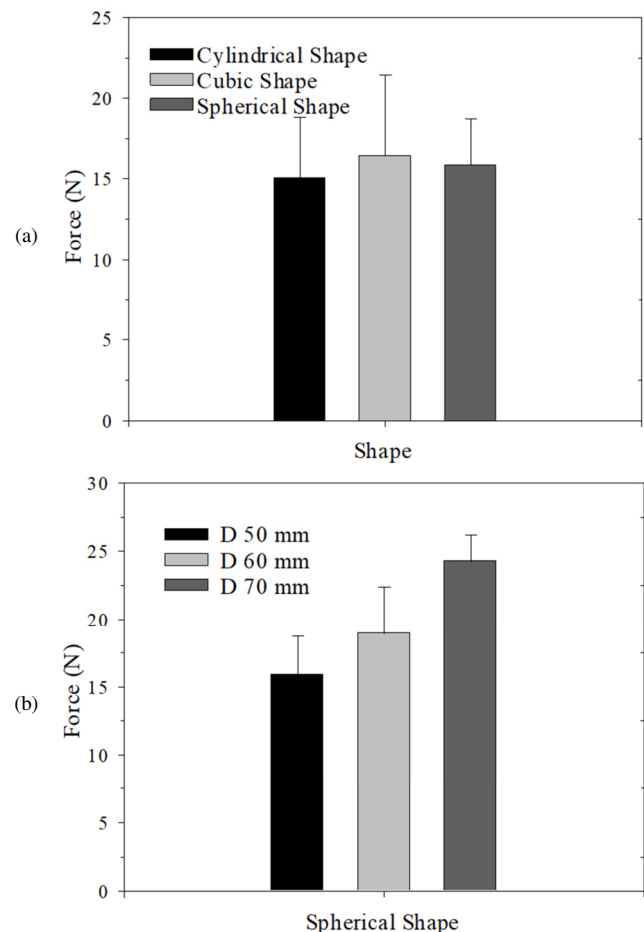


Fig. 14. Relationship between shape and force: (a) difference in object shape; (b) spherical shape with difference in diameter.

C. Grasping for Daily Life Objects

In this evaluation, the gripper's performance is examined in the context of object manipulation. The experimental apparatus consists of a diverse set of objects, including six distinct types

of fruits varying in size and weight, along with seven different everyday items characterized by varied sizes and weights. The total number of objects is 13, as shown in Figure 15.



Fig. 15. Daily life objects for grasping experiments.

The gripper is affixed to the end of a robotic arm for the experimental setup. During these trials, the air pressure is set to 30 kPa, and the gripper securely grasps each object for a duration of 10 seconds. The test entails the collection of objects

situated at a comparable level to that of a real-world scenario in which fruits are found growing on trees suspended above the ground.

The objects included in the evaluation spanned a broad spectrum, ranging from lightweight screwdrivers to larger multimeters. The fruits selected for the testing process exhibited diameters within the range of 50 mm to 85 mm. This comprehensive testing approach enables a thorough examination of the gripper's capacity to handle objects of varying sizes, weights, and characteristics as presented in Figure 16. The ensuing test results, as delineated in Table I, evince the gripper's aptitude in manipulating a diverse array of objects, exhibiting variances in dimensions and mass. However, exceptions were observed in the case of screwdrivers and remotes. The challenges encountered with these objects stem from the gripper's inherent behavior when subjected to opposing stretching forces. This behavior manifests as the formation of a minute circular gap, impeding the manipulation of objects with small diameters, such as screwdrivers. A similar issue arises when handling remotes due to their smooth surfaces, which limits surface contact and compromises the gripper's grip.

D. Harvesting Mangosteen

The present study aims to evaluate the effectiveness of soft grippers in mangosteen harvesting. To this end, an experiment was conducted in which mangosteens of various sizes and ripeness levels were categorized into four color stages: Level 1 (unripe) to Level 4 (fully ripe and ready for consumption).

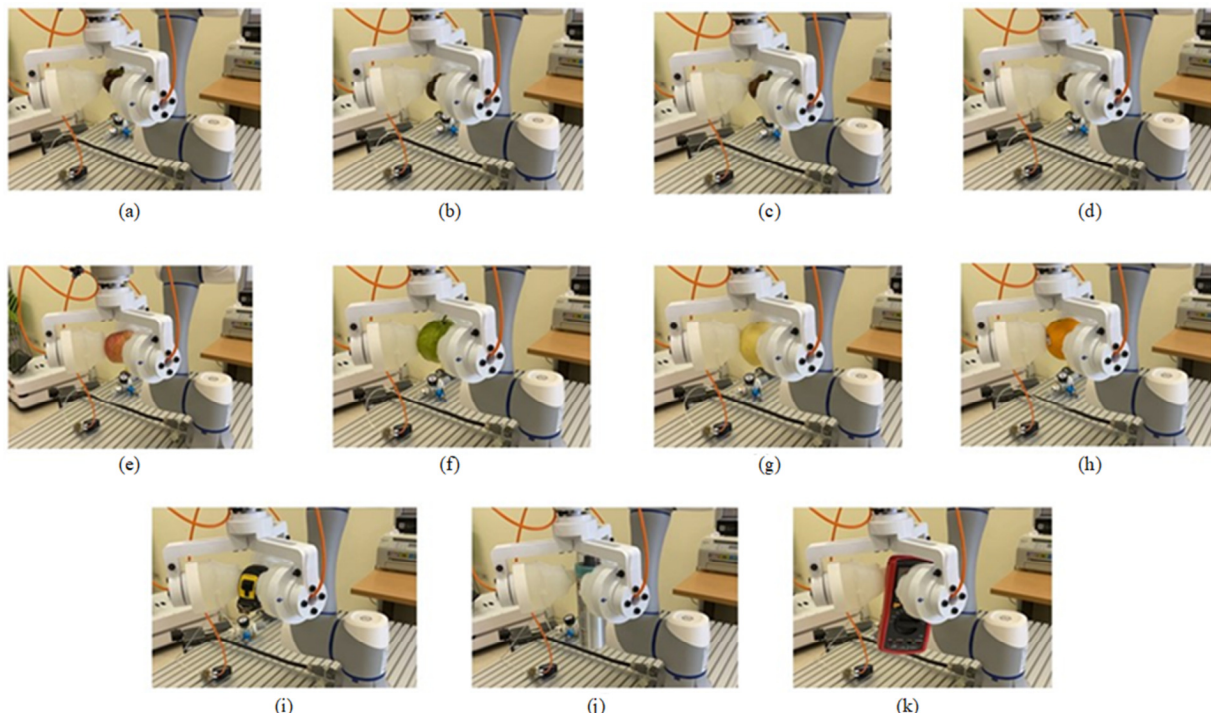


Fig. 16. Example of daily life objects grasping (a) mangosteen1, (b) mangosteen2, (c) mangosteen3, (d) mangosteen4, (e) apple, (f) guava, (g) pear, (h) orange, (i) tape measure, (j) can, and (k) multimeter.

The present study compares the harvesting performance of the soft gripper to that of traditional farming methods, focusing on the harvesting time. The soft gripper is affixed to the distal end of a retractable pole, as shown in Figure 17. An air compressor is employed to supply the requisite pressure for the harvesting process.

TABLE I. OBJECTS USED DURING THE GRASPING EXPERIMENT

Object	Mass (g)	Dimension (mm)	Success
Apple	190	72.1	Yes
Guava	306.2	85.2	Yes
Orange	207.8	83.9	Yes
Mangosteen 1	101.1	62.5	Yes
Mangosteen 2	66.1	50	Yes
Mangosteen 3	61.9	51.9	Yes
Mangosteen 4	62.2	50.9	Yes
Can	121	53×195	Yes
Screwdriver	81.1	24×116	No
Tape measure	380.8	78×81×83	Yes
Remote	116.2	26×47×145	No
Multimeter	556.9	56×95×195	Yes



Fig. 17. Operation of mangosteen harvesting equipment: in use during harvesting (left), harvesting at elevated heights (right).

As presented in Figure 18 (a), the harvesting of mangosteens at color level 1 requires a maximum of 7 seconds. This is due to the fact that level 1 signifies unripe green mangosteens with hard fruit stalks, which renders them more difficult to harvest. Conversely, harvesting mangosteens at color level 4, which signifies full ripeness with softer, black fruit stalks, requires a mere 4 seconds due to the weakened stalks, resulting in a more straightforward harvesting process. A comparison of harvesting times between soft grippers and farmers at the same color level as shown in Figure 18 (b) reveals that for color level 2, soft grippers require 5 seconds, while farmers take 7 seconds. This discrepancy can be attributed to the bamboo tools used by farmers, which have a higher propensity to slip on strong stalks, thereby prolonging the harvesting process. Conversely, at color levels 3 and 4, farmers exhibit higher efficiency compared to soft grippers, a phenomenon that is presumably attributable to their expertise and manual dexterity in manipulating ripe mangosteens. The telescopic soft gripper has demonstrated promising results in controlled environments, successfully handling mangosteen

fruits of varying sizes without causing damage. However, when considering real-world harvesting conditions, limitations emerge with respect to obstacle interference and limited posture adjustments. The gripper necessitates a substantial open space for the purpose of approach and departure. The presence of obstacles, such as branches, twigs, or leaves, between the target and the gripper has the potential to impede the effective retrieval of fruit. Addressing this limitation is imperative for the advancement of the gripper design. Subsequent iterations of the gripper design will be equipped with advanced sensing technologies and obstacle-avoidance algorithms to address this limitation.

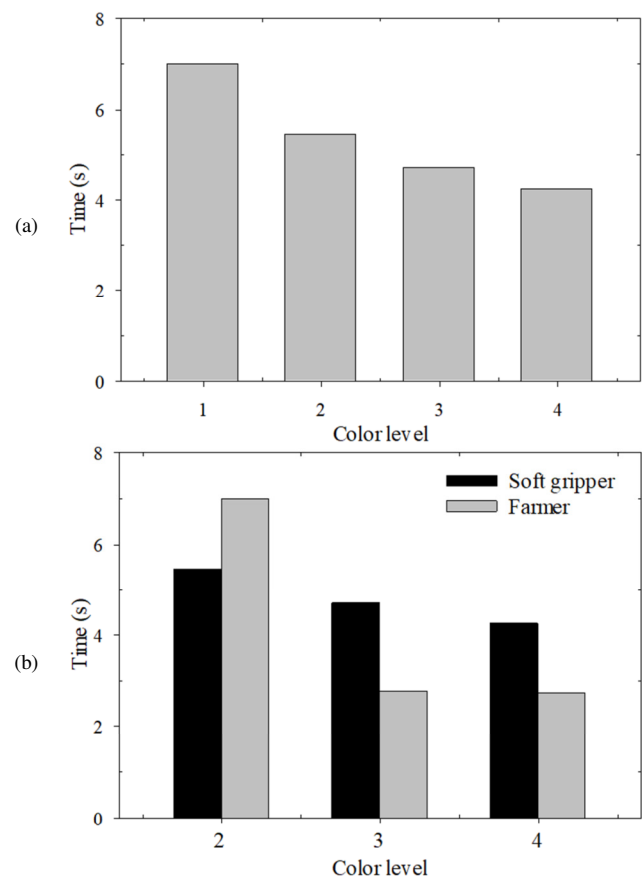


Fig. 18. (a) Relationship between harvesting time and mangosteen color levels, (b) comparison of harvesting times between farmers and soft grippers across different mangosteen color levels.

These enhancements are intended to improve the gripper's navigation in complex environments, thereby increasing its practicality in commercial settings. However, the current design lacks the necessary range for posture adjustments, thereby constraining its operational capacity in complex environments. For instance, while the gripper can easily grasp a suspended mangosteen, it encounters difficulties with fruits positioned at irregular angles or in confined spaces. Subsequent research will concentrate on incorporating an adaptive wrist mechanism or multi-axis rotation capability into the gripper's base to enhance its dexterity. In comparison to existing soft gripper designs, the proposed telescopic gripper demonstrates

superior flexibility and adaptability. For instance, it has been observed to outperform rigid grippers when handling delicate fruits, such as mangosteen, but exhibits deficiencies in environments characterized by high-density foliage. These findings underscore the trade-offs inherent in gripper design and underscore the need for continued innovation in this field.

V. CONCLUSIONS

Telescopic soft grippers have been designed to manipulate objects of diverse weights and dimensions. This is achieved by modifying critical parameters such as thickness and internal angle, enhancing their efficacy. The present study sought to enhance the design of the telescopic actuator by assessing nine distinct models with differing thicknesses and internal angles through the use of Finite Element Analysis (FEM). The model with a thickness of 2.25 mm and an internal tilt of 10 degrees demonstrated optimal performance, exhibiting the greatest stretchability with the least amount of stress when compared to other designs. A comparison of simulated and experimental findings revealed a high degree of agreement when air pressure was increased. An experiment was conducted to assess the gripper's resistance when manipulating objects of varying shapes and sizes. The results of this experiment demonstrated that adhesion forces fluctuated according to the shape and size of the items, with larger and more curved objects displaying enhanced adherence. The performance of the gripper was evaluated by handling fruits and various objects encountered in daily life at 20 kPa. The gripper exhibited proficiency in handling objects of diverse dimensions and mass, with the exception of small, smooth objects such as screwdrivers and remotes, which resulted in limited grip surface. Finally, a mangosteen harvesting experiment evaluated the gripper's efficiency in picking fruit at different ripeness levels and compared its performance to that of traditional farmers. The grapple harvested mangosteens at color level 2 faster, but was slower at levels 3 and 4. However, the gripper's need for an unobstructed working environment and its limited ability to change posture make it difficult to use. For future work, the telescoping soft gripper is needed to create a more compact gripper capable of picking mangosteens while avoiding obstacles such as branches and leaves. This device will be integrated with a robotic arm to facilitate harvesting and replace human labor, and image analysis software will be used to assist in sorting mangosteens by size and color grade. In addition, integrating information from recent developments in robotic systems and multi-agent reinforcement learning could improve the efficiency and adaptability of automated harvesting techniques.

ACKNOWLEDGMENT

This work (Grant No. RGNS 65-197) was supported by the Office of the Permanent Secretary, Ministry of Higher Education, Science, Research, and Innovation (OPS MHESI), Thailand Science Research and Innovation (TSRI), and Faculty of Engineering, Prince of Songkla University, Thailand.

REFERENCES

- [1] Y. Hua *et al.*, "Recent Advances in Intelligent Automated Fruit Harvesting Robots," *The Open Agriculture Journal*, vol. 13, no. 1, pp. 101–106, Aug. 2019, <https://doi.org/10.2174/1874331501913010101>.
- [2] K. Jha, A. Doshi, P. Patel, and M. Shah, "A comprehensive review on automation in agriculture using artificial intelligence," *Artificial Intelligence in Agriculture*, vol. 2, pp. 1–12, Jun. 2019, <https://doi.org/10.1016/j.aiaa.2019.05.004>.
- [3] S. Kappagantula, G. Mannayee, A. S. Veerendra, S. Dutta, and A. Flah, "Enhancing the Structural Integrity and Performance of an Agricultural Robot with Caterpillar Tracks: A Comprehensive Deformation Analysis," *Engineering, Technology & Applied Science Research*, vol. 14, no. 4, pp. 15910–15915, Aug. 2024, <https://doi.org/10.48084/etasr.7740>.
- [4] A. L. Gunderman, J. A. Collins, A. L. Myers, R. T. Threlfall, and Y. Chen, "Tendon-Driven Soft Robotic Gripper for Blackberry Harvesting," *IEEE Robotics and Automation Letters*, vol. 7, no. 2, pp. 2652–2659, Apr. 2022, <https://doi.org/10.1109/LRA.2022.3143891>.
- [5] A. De Preter, J. Anthonis, and J. De Baerdemaeker, "Development of a Robot for Harvesting Strawberries," *IFAC-PapersOnLine*, vol. 51, no. 17, pp. 14–19, Jan. 2018, <https://doi.org/10.1016/j.ifacol.2018.08.054>.
- [6] X. Wang, H. Kang, H. Zhou, W. Au, M. Y. Wang, and C. Chen, "Development and evaluation of a robust soft robotic gripper for apple harvesting," *Computers and Electronics in Agriculture*, vol. 204, Jan. 2023, Art. no. 107552, <https://doi.org/10.1016/j.compag.2022.107552>.
- [7] C.-H. Liu, C.-H. Chiu, T.-L. Chen, T.-Y. Pai, Y. Chen, and M.-C. Hsu, "A Soft Robotic Gripper Module with 3D Printed Compliant Fingers for Grasping Fruits," in *2018 IEEE/ASME International Conference on Advanced Intelligent Mechatronics (AIM)*, Auckland, New Zealand, Jul. 2018, pp. 736–741, <https://doi.org/10.1109/AIM.2018.8452420>.
- [8] R. Goulart, D. Jarvis, and K. B. Walsh, "Evaluation of End Effectors for Robotic Harvesting of Mango Fruit," *Sustainability*, vol. 15, no. 8, Jan. 2023, Art. no. 6769, <https://doi.org/10.3390/su15086769>.
- [9] G. Gao, C.-M. Chang, L. Gerez, and M. Liarokapis, "A Pneumatically Driven, Disposable, Soft Robotic Gripper Equipped With Multi-Stage, Retractable, Telescopic Fingers," *IEEE Transactions on Medical Robotics and Bionics*, vol. 3, no. 3, pp. 573–582, Aug. 2021, <https://doi.org/10.1109/TMRB.2021.3097143>.
- [10] M. Azizkhani, A. Sangsefidi, J. Kadkhodapour, and A. P. Anaraki, "Numerical and experimental investigation for monitoring and prediction of performance in the soft actuator," *Structural Engineering and Mechanics*, vol. 77, no. 2, pp. 167–177, 2021, <https://doi.org/10.12989/sem.2021.77.2.167>.
- [11] Z. Long, Q. Jiang, T. Shuai, F. Wen, and C. Liang, "A Systematic Review and Meta-analysis of Robotic Gripper," *IOP Conference Series: Materials Science and Engineering*, vol. 782, no. 4, Mar. 2020, Art. no. 042055, <https://doi.org/10.1088/1757-899X/782/4/042055>.
- [12] A. K. Jaiswal and B. Kumar, "Vacuum Gripper-An important material handling tool," *International Journal of Science & Technology*, vol. 7, no. 1, pp. 1–8, Feb. 2017.
- [13] S. Li *et al.*, "A Vacuum-driven Origami 'Magic-ball' Soft Gripper," in *2019 International Conference on Robotics and Automation (ICRA)*, Montreal, QC, Canada, May 2019, pp. 7401–7408, <https://doi.org/10.1109/ICRA.2019.8794068>.
- [14] Y. Cui, X.-J. Liu, X. Dong, J. Zhou, and H. Zhao, "Enhancing the Universality of a Pneumatic Gripper via Continuously Adjustable Initial Grasp Postures," *IEEE Transactions on Robotics*, vol. 37, no. 5, pp. 1604–1618, Oct. 2021, <https://doi.org/10.1109/TRO.2021.3060969>.
- [15] L. Gerez, C.-M. Chang, and M. Liarokapis, "A Hybrid, Encompassing, Three-Fingered Robotic Gripper Combining Pneumatic Telescopic Mechanisms and Rigid Claws," in *2020 IEEE International Symposium on Safety, Security, and Rescue Robotics (SSRR)*, Nov. 2020, pp. 142–147, <https://doi.org/10.1109/SSRR50563.2020.9292622>.
- [16] H. Ji, L. Zhang, S. Nie, L. Huo, S. Nie, and Z. Wu, "Optimization design and experiment study on a water hydraulic flexible actuator integrating flexible inner skeleton and soft external skin used for underwater flexible gripper," *Sensors and Actuators A: Physical*, vol. 366, Feb. 2024, Art. no. 114957, <https://doi.org/10.1016/j.sna.2023.114957>.
- [17] S. Zhou, C. Shen, F. Pang, Z. Chen, J. Gu, and S. Zhu, "Position-Based Visual Servoing Control for Multi-Joint Hydraulic Manipulator," *Journal of Intelligent & Robotic Systems*, vol. 105, no. 2, May 2022, Art. no. 33, <https://doi.org/10.1007/s10846-022-01628-x>.

- [18] N. Shewale and R. Deivanathan, "Modelling and analysis of dc motor actuator for an electric gripper," *Journal of Engineering Science and Technology*, vol. 13, no. 4, pp. 862–874, 2018.
- [19] M. E. M. Salem, Q. Wang, R. Wen, and M. Xiang, "Design and Characterization of Soft Pneumatic Actuator for Universal Robot Gripper," in *2018 International Conference on Control and Robots (ICCR)*, Hong Kong, China, Sep. 2018, pp. 6–10, <https://doi.org/10.1109/ICCR.2018.8534483>.
- [20] K. C. Galloway *et al.*, "Soft Robotic Grippers for Biological Sampling on Deep Reefs," *Soft Robotics*, vol. 3, no. 1, pp. 23–33, Mar. 2016, <https://doi.org/10.1089/soro.2015.0019>.
- [21] G. P. Kontoudis, M. V. Liarakapis, A. G. Zisimatos, C. I. Mavrogiannis, and K. J. Kyriakopoulos, "Open-source, anthropomorphic, underactuated robot hands with a selectively lockable differential mechanism: Towards affordable prostheses," in *2015 IEEE/RSJ International Conference on Intelligent Robots and Systems (IROS)*, Hamburg, Germany, Sep. 2015, pp. 5857–5862, <https://doi.org/10.1109/IROS.2015.7354209>.
- [22] R. Ma and A. Dollar, "Yale OpenHand Project: Optimizing Open-Source Hand Designs for Ease of Fabrication and Adoption," *IEEE Robotics & Automation Magazine*, vol. 24, no. 1, pp. 32–40, Mar. 2017, <https://doi.org/10.1109/MRA.2016.2639034>.
- [23] P. Bharath Vamsi and V. Ragavendra Rao, "Design and fabrication of soft gripper using 3D printer," *IOP Conference Series: Materials Science and Engineering*, vol. 402, no. 1, Aug. 2018, Art. no. 012026, <https://doi.org/10.1088/1757-899X/402/1/012026>.
- [24] M. Liu, L. Hao, W. Zhang, and Z. Zhao, "A novel design of shape-memory alloy-based soft robotic gripper with variable stiffness," *International Journal of Advanced Robotic Systems*, vol. 17, no. 1, Jan. 2020, Art. no. 1729881420907813, <https://doi.org/10.1177/1729881420907813>.
- [25] R. Konda, D. Bombara, S. Swanbeck, and J. Zhang, "Anthropomorphic Twisted String-Actuated Soft Robotic Gripper With Tendon-Based Stiffening," *IEEE Transactions on Robotics*, vol. 39, no. 2, pp. 1178–1195, Apr. 2023, <https://doi.org/10.1109/TRO.2022.3224774>.
- [26] J.-H. Lee, Y. S. Chung, and H. Rodrigue, "Long Shape Memory Alloy Tendon-based Soft Robotic Actuators and Implementation as a Soft Gripper," *Scientific Reports*, vol. 9, no. 1, Aug. 2019, Art. no. 11251, <https://doi.org/10.1038/s41598-019-47794-1>.
- [27] J.-Y. Lee *et al.*, "Shape-Adaptive Universal Soft Parallel Gripper for Delicate Grasping Using a Stiffness-Variable Composite Structure," *IEEE Transactions on Industrial Electronics*, vol. 68, no. 12, pp. 12441–12451, Dec. 2021, <https://doi.org/10.1109/TIE.2020.3044811>.
- [28] D. Sui *et al.*, "A Bioinspired Soft Swallowing Gripper for Universal Adaptable Grasping," *Soft Robotics*, vol. 9, no. 1, pp. 36–56, Feb. 2022, <https://doi.org/10.1089/soro.2019.0106>.
- [29] J. H. Shin, J. G. Park, D. I. Kim, and H. S. Yoon, "A Universal Soft Gripper with the Optimized Fin Ray Finger," *International Journal of Precision Engineering and Manufacturing-Green Technology*, vol. 8, no. 3, pp. 889–899, May 2021, <https://doi.org/10.1007/s40684-021-00348-1>.
- [30] J. Auyasakul, A. Booranawong, N. Vittayaphadung, and P. Smithmaitrie, "An Optimized Design of the Soft Bellow Actuator Based on the Box-Behnken Response Surface Design," *Actuators*, vol. 12, no. 7, Jul. 2023, Art. no. 300, <https://doi.org/10.3390/act12070300>.
- [31] E. Navas, R. Fernández, M. Armada, and P. Gonzalez-de-Santos, "Diaphragm-Type Pneumatic-Driven Soft Grippers for Precision Harvesting," *Agronomy*, vol. 11, no. 9, Sep. 2021, Art. no. 1727, <https://doi.org/10.3390/agronomy11091727>.